General Disclaimer

One or more of the Following Statements may affect this Document

- This document has been reproduced from the best copy furnished by the organizational source. It is being released in the interest of making available as much information as possible.

- This document may contain data, which exceeds the sheet parameters. It was furnished in this condition by the organizational source and is the best copy available.

- This document may contain tone-on-tone or color graphs, charts and/or pictures, which have been reproduced in black and white.

- This document is paginated as submitted by the original source.

- Portions of this document are not fully legible due to the historical nature of some of the material. However, it is the best reproduction available from the original submission.

SEMI-ANNUAL PROGRESS REPORT

covering the period

1 September 1975 to 29 February 1976

for

GRANT NSG-2075

entitled

PROPERTIES OF THE MOON AND ITS ENVIRONMENT FROM LUNAR MAGNETOMETER MEASUREMENTS

Conducted by

Curtis W. Parkin
Principal Investigator

Department of Physics
University of Santa Clara
California 95053

The NASA Technical Officer for this grant is

Dr. P. Dyal, Astrophysics Branch,
NASA-Ames Research Center, Moffett Field, CA 94035

I. INTRODUCTION

This is a six-month progress report covering research on the moon and its environment by the principal investigator. The specific objectives, approaches, and statements of work are presented in the body of the proposal submitted in February 1975. Section II briefly summarizes results in the primary research areas, and Section III lists publications and verbal papers submitted during the six-month period. Copies of publications and abstracts are included in Section IV.

II. SUMMARY OF RESULTS

During the time period 1 September 1975 - 28 February 1976 our lunar analysis has expanded to include data from a total of nine lunar magnetometers: three Apollo lunar surface magnetometers, two Apollo subsatellite magnetometers, two magnetometers aboard Explorer 35, and the Russian Luna-22 orbiter and Lunokhod-2 surface rover. New results have been obtained concerning electromagnetic, compositional, and structural properties of the lunar interior. In particular, the following tasks were completed during the grant period.

(1) Lunar Magnetic Permeability and Iron Abundance: Recent research studying magnetic permeability and iron abundance of the moon has involved the use of two different analytical techniques and a total of five different instruments. In the first technique simultaneous data are used from one Apollo surface magnetometer and one or both magnetometers aboard the lunar orbiting Explorer 35. A total of 10 lunations of quiet geomagnetic tail data have been used, extending over parts of 3 different calendar years.

In the second (more recent) technique we use 5 lunations of simultaneous data from two Apollo surface magnetometers. This technique uses a differential method of subtracting out the external magnetizing field and has the

advantages of (a) using all three vector components in the analysis rather than just the radial component, (b) subtracting out all constant fields measured out at either site, making its analysis independent of offset errors and remanent field determination at either site, and (c) making use of high resolution LSM data only. The table below summarizes magnetic permeability results to date.

Magnetometers	No. Lunations	Date	Components Used	Permeability
AP 12 LSM/EX 35	8	1969-70	Radial only	1.012±0.006
AP 15 LSM/EX 35	2	1971	Radial only	1.019±0.004
AP 15 LSM/AP 16 LSM	5	1972	all	1.008±0.005

We are able to calculate iron abundance in the moon from the bulk lunar permeability by assuming a suitable mineral compositional model of the moon (olivine or orthopyroxene of density and percentage iron silicate composition consistent with known global density, moment of inertia & other geochemical constraints); and a Curie isotherm depth consistent with lunar temperature profiles determined by seismic, magnetometer, and geochemical results. The free iron content is found to be 2.5 ± 2.0 percent by weight and the total iron in the moon is 9.0 ± 4.7 wt %.

(2) Limits on a Highly-Conducting Lunar Core: The moon could have a small highly conducting lunar core which, if having a sufficiently long Cowling time of the order of a few days or longer, would continually exclude the external geomagnetic tail field, therefore acting as a "diamagnetic" region of effective permeability = 0. In this case the field enhancement of the outer region dominated by ferromagnetic and paramagnetic iron would

compete with the field decrease of the "diamagnetic" core; magnetometers on the surface or in lunar orbit would then measure the resultant net field. Our previously reported results assumed no such diamagnetic core; indeed, nothing in our permeability or conductivity studies indicates the existence of such a core.

A preliminary calculation of the upper limits on the size of a highly conducting (assumed $\sigma = \infty$) core has been completed for an assumed Curie isotherm depth of 250 km (consistent with electrical conductivity results). We have calculated two cases for lunar compositions of olivine and orthopyroxene, in each case assuming no iron silicate, so that free iron content is maximized and therefore size of the hypothetical core is maximized. The upper limit on an orthopyroxene moon is 535 km and for an olivine moon 385 km. It is noted that for both lunar models the minimum core radius is zero, that is, all our measurements to date are consistent with the nonexistence of a highly conducting core.

(3) Lunar Electrical Conductivity: A new analytical technique has been recently developed and applied to lunar electrical conductivity, in which simultaneous data measured in high-latitude regions of the geomagnetic tail are used from a network of three instruments: the Apollo 15 lunar surface magnetometer (LSM), the Apollo 16 LSM, and the Apollo 16 subsatellite magnetometer, which provides coverage around the entire global circumference. A numerical analysis program uses measured total fields from the three magnetometers to separate the time-varying field from the induced lunar poloidal eddy current field. Thereafter a conductivity profile for the lunar interior can be found by an iterative technique.

Also, a two-instrument technique has been applied which uses Apollo 12 LSM data and simultaneous data from the Goddard magnetometer aboard Explorer 35. All measurements are made when the moon is located in high-latitude regions of the geomagnetic tail where plasma effects in the lunar environment are minimal. Individual magnetic events are superimposed to obtain a single large transient for analysis. Also, during examination of five years of data one exceptionally large, well-behaved transient was recorded when the moon was in the geomagnetic tail. This single event promises substantial improvement in resolution and sounding depth for conductivity analysis. Most recent electrical conductivity results are included in Section IV.

(4) Lunar Internal Structure Inferred from Conductivity and Permeability Results: Structural implications of conductivity results to date (Dyal et al., 1976) are as follows: The first 250 km depth has very low electrical conductivity. No conductivity transition is seen at the 60 km seismic discontinuity reported by Nakamura, Latham and coworkers, but our resolution to date is limited at such shallow depths. Between 250-300 km depth the conductivity increases dramatically, reaching a "knee" at about 300 km depth. This change corresponds closely to the seismic discontinuity at that depth. From 300-900 km depth the conductivity continues increasing, but at a decreased rate. At about 900 km a slight increase in conductivity is indicated by the best fit profile at the seismic velocity change in the moon quake region of the lunar interior, but errors on the conductivity profile are large enough at these depths to prevent a definite conclusion at this time. A highly conducting core of maximum radius 535 km is found to be possible for the extreme case of magnesium-silicate dominated orthopyroxene with Curie isotherm depth

of 250 km indicated from the temperature profiles inferred from conductivity calculations. However, there is no positive indication at this time that any core of conductivity > 10 mho/m need exist in the moon.

III. LIST OF PUBLICATIONS/ABSTRACTS

(1) Dyal P., Parkin C.W., and Daily W.D., "Lunar Electrical Conductivity and Magnetic Permeability." Proc. Lunar Sci. Conf., 6th, vol. 3, pp. 2909-2926, 1975. Pergamon Press.

(2) Dyal P., Parkin C.W., and Daily W.D., "Structure of the Lunar Interior from Magnetic Field Measurements," in Lunar Science VII, part I, 1976.

(3) Daily W.D., Dyal P., and Parkin C.W., "Lunar Electrical Conductivity Profile from Magnetometer Network," (abs.) to be published in EOS, vol. 57, 1976.

IV. PUBLICATIONS AND ABSTRACTS

Proc. Lunar Sci. Conf. 6th (1975), p. 2909–2926.
Printed in the United States of America

Lunar electrical conductivity and magnetic permeability

PALMER DYAL

NASA Ames Research Center, Moffett Field, California 94035

CURTIS W. PARKIN

Department of Physics, University of Santa Clara, Santa Clara, California 95053

WILLIAM D. DAILY

Department of Physics and Astronomy, Brigham Young University, Provo, Utah 84602

Abstract—Improved analytical techniques are applied to a larger Apollo magnetometer data set to yield values of electrical conductivity, temperature, magnetic permeability, and iron abundance. Average bulk electrical conductivity of the moon is calculated to be 7×10^{-4} mho/m. Allowable solutions for electrical conductivity indicate a rapid increase with depth to $\sim 10^{-3}$ mho/m within 250 km. The upper limit on the calculated size of a hypothetical highly conducting core ($\geq 7 \times 10^{-3}$ mho/m) is $0.57 R/R_{moon}$. The temperature profile, obtained from the electrical conductivity profile using the laboratory data of Duba *et al.* (1974) for olivine, indicates high lunar temperatures at relatively shallow depths. These results imply that the Curie isotherm is at a depth of less than 200 km. Magnetic permeability of the moon relative to its environment is calculated to be 1.008 ± 0.005. Adjustment of this result to account for a diamagnetic lunar ionosphere yields a lunar permeability, relative to free space, of $1.012^{+0.011}_{-0.008}$. Lunar iron abundances corresponding to this permeability value are $2.5^{+2.3}_{-1.7}$ wt.% free iron, and 5.0–13.5 wt.% total iron for a moon composed of a combination of free iron, olivine, and orthopyroxene.

INTRODUCTION

DATA FROM the network of magnetometers placed on the moon by Apollo astronauts have allowed investigation of internal lunar properties. The purpose of this paper is to report our latest results of lunar electrical conductivity, temperature, magnetic permeability, and iron abundance.

Previous electrical conductivity analyses using a time-dependent transient response technique have been applied to nightside lunar data with the moon in the solar wind (e.g., Dyal and Parkin, 1971a; Dyal *et al.*, 1972), dayside data in the solar wind (Dyal *et al.*, 1973), and to geomagnetic tail data (Dyal *et al.*, 1974). Results to be presented here are calculated using data from deep in the geomagnetic tail lobes. A new transient-superposition technique is used which improves the signal-to-noise ratio in the analysis. In addition, amplitude and phase information are used for all three vector components of magnetic field data.

In our earlier work on magnetic permeability and iron abundance of the moon (Dyal and Parkin, 1971b; Parkin *et al.*, 1973, 1974), the analytical technique involved use of simultaneous data from the lunar orbiting Explorer 35 magnetometer and the Apollo 12 or 15 surface magnetometer. With the present

technique, simultaneous data from the Apollo 15 and 16 surface magnetometers are used, requiring no orbital magnetic field data. This method has the advantages of using only the higher resolution surface magnetometers, and is insensitive to instrument offsets. The lunar ionosphere in the geomagnetic tail is modeled, and results are compared with those of Apollo subsatellite measurements (Russell *et al.*, 1974a,b). Values of lunar magnetic permeability and iron abundance are calculated taking into account effects of the diamagnetic ionosphere.

LUNAR ELECTRICAL CONDUCTIVITY AND TEMPERATURE

Lunar electrical conductivity is calculated using measurements of global eddy current fields induced by changes in the magnetic field external to the moon. The time dependence of the induced field response is a function of the electrical conductivity distribution in the lunar interior. Simultaneous measurements of the transient driving field and the lunar response field, by Explorer 35 and Apollo surface magnetometers, allow calculations of the conductivity. Detailed descriptions of the Apollo and Explorer 35 instruments are reported in Dyal *et al.* (1970) and Sonett *et al.* (1967).

Analytical technique

Data have been selected from measurements obtained in the lobes of the geomagnetic tail, during times when there is no indication of plasma effects (Anderson, 1965). The individual data sets are also subject to the following data selection criteria: (1) the magnitude of the field external to the moon (measured by the Explorer 35 magnetometer) is required to be at all times greater than 8 gammas; (2) the external field is directed approximately along the sun-earth line; (3) main qualitative features of each event are required to appear in both surface and orbital data in all three vector coordinate axes to minimize use of data with large field gradients between the two magnetometers; and (4) no plasma data are measured above the solar-wind spectrometer instrument threshold. Criteria (1) and (2) are used to insure that no neutral sheet crossings are used in the analysis. Therefore, we have chosen data for times when the lunar response can be modeled by that of a conducting sphere in a vacuum. Details of the vacuum theory are reported in Dyal *et al.* (1972, 1974).

Since the field equations governing the electromagnetic response of a sphere in a vacuum are linear, the sum of any two solutions is itself a solution. We take advantage of this principle by superimposing many driving functions (measured by the Explorer 35 orbiting magnetometer) to form an aggregate data event, and comparing this with the aggregate formed by superposition of the corresponding response functions (measured by an Apollo surface magnetometer). These aggregates have much higher signal-to-noise characteristics than do the individual events since errors such as those due to magnetometer digitization and to geotail gradients will be gaussian and tend to average out in the event-addition process. The response to the driving field aggregate is calculated for an assumed electrical

conductivity profile $\sigma(r)$, compared to the measured time series response (Apollo magnetometer data aggregate) and then reiterated by adjusting $\sigma(r)$ until the error between the calculated response and measured response is minimized.

Electrical conductivity results

The eighteen data events used in our analysis have been linearly superimposed using a 20-inch IMLAC programmable display system in a real-time interactive mode with the Ames IBM 360/67 computer. For an assumed conductivity profile the IMLAC display is used to compare the calculated response with the measured Apollo aggregate. The conductivity profile is then iteratively adjusted until the calculated response function matches the measured Apollo response. Transient aggregates for the radial and two tangential axes are shown in Figs. 1, 2, and 3. The "computer response field" in each of these figures is calculated from the conductivity profile displayed in Fig. 4. The figure insert shows a family of profiles which also fit the data and give bounds on lunar conductivity. One of the profiles shown in the insert is the homogeneous-moon profile, which gives a value of 7×10^{-4} for the average bulk conductivity of the moon.

In our analysis we assume that the electrical conductivity increases monotonically with depth from 10^{-9} mho/m at the surface (Dyal and Parkin, 1971b) and that

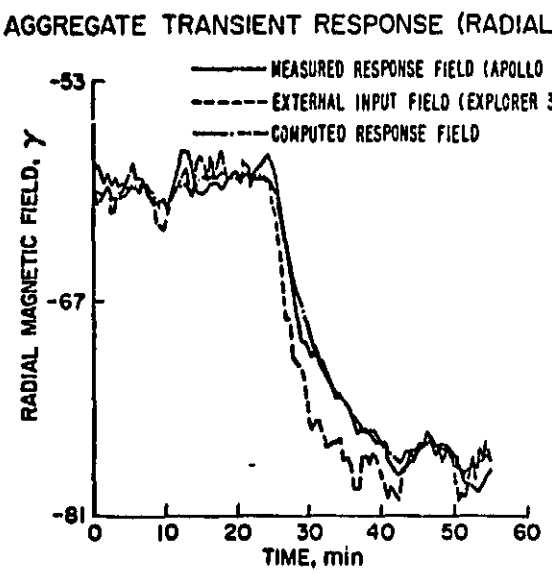

Fig. 1. Aggregate transient response (radial-x). The aggregate is the sum of radial (ALSEP x-axis) magnetic field components for eighteen events in the geomagnetic tail lobes, selected to minimize plasma effects. The external field is a sum of events measured by lunar orbiting Explorer 35 magnetometer; measured response field is the surface magnetic field aggregate of the same events measured by the Apollo 12 magnetometer. Computed response field is a theoretical response calculated for a sphere of electrical conductivity $\sigma(r)$ shown in Fig. 4.

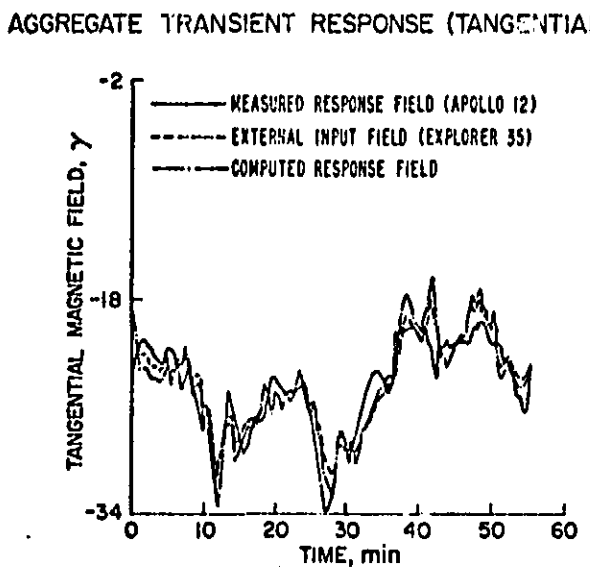

Fig. 2. Aggregate transient response (tangential-y). Aggregates are the external, computed, and measured response fields for the tangential (eastward) ALSEP *Y*-axis corresponding to the radial *X*-axis data illustrated in Fig. 1.

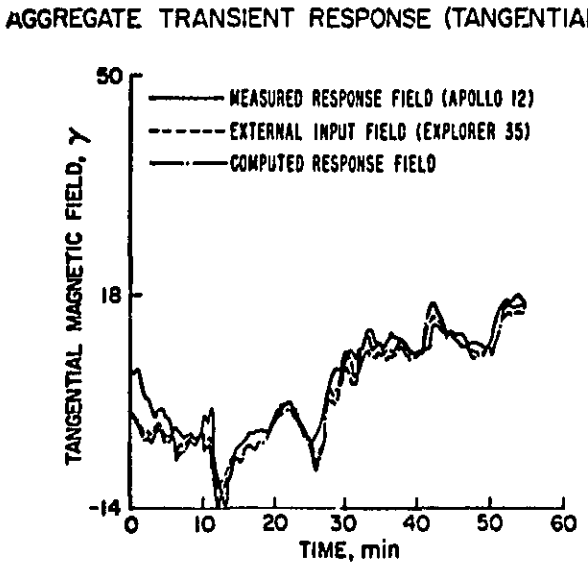

Fig. 3. Aggregate transient response (tangential-z). Aggregates are the external, computed, and measured response fields for the tangential (northward) ALSEP *Z*-axis corresponding to the radial *X*-axis data illustrated in Fig. 1.

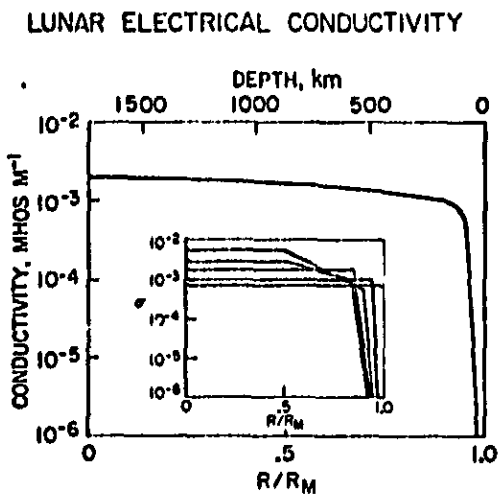

Fig. 4. Lunar electrical conductivity profile which gives "best-fit" response to the aggregate event shown in Figs. 1, 2, and 3. Insert shows other conductivity profiles which give approximate bounds on the range of allowed solutions.

it is a continuous function from the surface to the center of the moon. (The conductivity is shown for all radii in Figs. 4 and 5 since the analysis requires that the conductivity be defined throughout the entire lunar sphere.) The uncertainty in the electrical conductivity is reflected in the spread of allowable profiles shown in Fig. 4 insert. These profiles are the simplest forms that we consider appropriate for our data set: the conductivity below $0.3R_m$, however, can vary by orders of magnitude without being discriminated by our technique. These uncertainties cannot be delineated by error bars associated with individual depths because errors in the analysis are reflected by the entire conductivity function. The uncertainty in the profile arises from several factors: (1) the nonuniqueness of

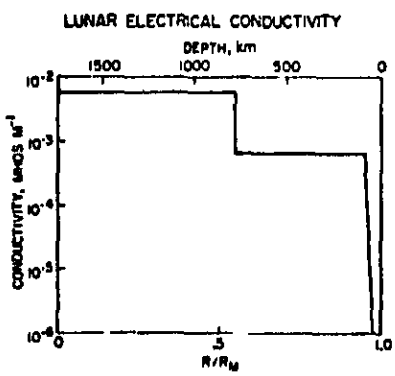

Fig. 5. Electrical conductivity profile illustrating the maximum size of a hypothetical highly conducting core of conductivity 7×10^{-1} mho/m: $R_{core} \leq 0.57R_m$.

profile determination as discussed by Backus and Gilbert (1970), Phillips (1972), and Hobbs (1973); (2) the penetration depth allowed by the length of the data set used and its frequency content; (3) the frequency response limitations of the Explorer 35 and Apollo magnetometers; (4) nonhomogeneities in the external field over the dimensions of the moon; and (5) instrumental errors in the measured fields. The conductivity profiles shown in Fig. 4 are consistent with previous transient-analysis results (Dyal and Parkin, 1971a; Dyal *et al.*, 1974).

An important result of this analysis is that the lunar conductivity rises rapidly to 10^{-3} mho/m within 250-km depth and remains relatively constant to 800-km depth. We have also investigated the possibility that a partially molten core exists in the moon at a depth of approximately 800 km, as indicated by seismic results (Nakamura *et al.*, 1974). We have examined the limits that electrical conductivity analysis places upon a partially molten core, using an order-of-magnitude increase in conductivity to represent a phase change (Khitarov *et al.*, 1970; Presnall *et al.*, 1972), then determining where such a highly conducting core could exist consistent with magnetic field data. The upper limit on the size of such a core is determined to be 0.57 lunar radius, close to the value $0.55R_{moon}$ determined from seismic measurements (Nakamura *et al.*, 1974). Analysis of longer transient-event aggregates will further define the size limit on a highly conducting core in the moon.

Inferred lunar temperature

For minerals which are probable constituents of the lunar interior, the electrical conductivity can be expressed as a function of temperature, and therefore a thermal profile of the lunar interior can be inferred from the conductivity profile in Fig. 3 for an assumed material composition. Many investigators have published laboratory results relating conductivity to temperature for materials which are geochemical candidates for the lunar interior (e.g., England *et al.*, 1968; Duba *et al.*, 1972; Schwerer *et al.*, 1972; Duba and Ringwood, 1973; Olhoeft *et al.*, 1973).

Recently Duba *et al.* (1974) have measured conductivity of olivine as a function of temperature under controlled oxygen fugacity and have found the measurements to be essentially pressure independent up to 8 kbar. These measurements for olivine have been used to convert our conductivity profile of Fig. 4 to a temperature profile (Fig. 6). The Fig. 6 insert shows a family of temperature profiles which reflect the error limits of our conductivity calculations. We see from Fig. 6 that the iron Curie isotherm (~780°C) should be reached within a depth of 200 km, allowing permanently magnetized material to exist only at shallow depths in the moon. The results imply a high temperature gradient to 250-km depth (averaging 6°K/km), and rather uniform temperature from 250 to 800-km depth. Similar conclusions have been reached by Kuckes (1974) using harmonic analysis of magnetometer data with the interpretation that convection is an important process in the present day moon. Also Hanks and Anderson (1972) have theoretically calculated a thin thermal boundary layer and high temperature interior for the moon, consistent with our results.

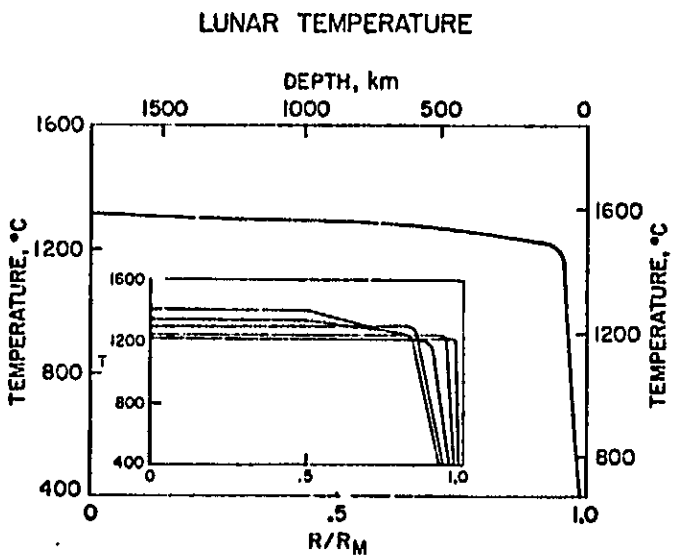

Fig. 6. Temperature profiles of the lunar interior, determined from the conductivity profiles in Fig. 4. A lunar interior composition of olivine is assumed; laboratory data for olivine from Duba *et al.* (1974) are used in the calculation.

Lunar Magnetic Permeability and Iron Abundance

Relative magnetic permeability of the moon can be calculated using data measured during times when the global magnetization field is the dominant induced lunar field. This type of induction dominates when the moon is in magnetically quiet regions of the geomagnetic tail, where the ambient external field is essentially constant and therefore eddy current induction is minimal.

Analytical technique

In previous reports (Parkin *et al.*, 1973, 1974) we calculated permeability μ using simultaneous measurements of the external field **H** by the lunar orbiting Explorer 35 magnetometer and the total surface field **B** using the Apollo 12 or 15 lunar surface magnetometer (LSM). In the present analytical method, simultaneous magnetic field data from Apollo 15 and 16 LSM's are used, requiring no orbital magnetometer data. This method has the advantages of (1) higher resolution of the LSM's and (2) results are not sensitive to instrument offsets, since calculations involve field differences, and offsets are canceled out of the analytical equations. Also, data are selected from deep in geomagnetic tail lobes where plasma effects are minimized, and 10-min averages of steady data are used so that eddy current induction effects are negligible.

Our present method involves using sets of field measurements **B** made at *two* times, each simultaneously at *two* Apollo sites (by the Apollo 15 and 16 LSM's). A description of the theoretical development is given in Appendix A. In this method

a system of twelve equations is used plus a transformation matrix relating fields measured at the two surface sites, yielding a total of 13 equations with 10 unknowns. These equations are solved for the lunar bulk relative magnetic permeability μ_b, expressed as follows:

$$\mu_b = \frac{\Delta B_{2x} - a_{11}\Delta B_{1x}}{a_{12}\Delta B_{1y} + a_{13}\Delta B_{1z}} \tag{1}$$

$$= \frac{a_{21}\Delta B_{1x}}{\Delta B_{2y} - a_{22}\Delta B_{1y} - a_{23}\Delta B_{1z}} \tag{2}$$

$$= \frac{a_{31}\Delta B_{1x}}{\Delta B_{2z} - a_{32}\Delta B_{1y} - a_{33}\Delta B_{1z}} \tag{3}$$

where subscripts 1 and 2 denote Apollo sites, e.g. site 1 can be designated Apollo 15 and site 2, Apollo 16; subscripts x, y, z, denote vector components in the ALSEP coordinate system with origin at either site, where $\hat{x}$ is directed radially outward from the lunar surface, and $\hat{y}$ and $\hat{z}$ are tangent to the surface, directed eastward and northward, respectively; a_{ij} is an element in the transformation matrix from site 1 to site 2. Each field-difference term $\Delta B_{ij} = B_{ij}(t_m) - B_{ij}(t_n)$ denotes a difference in a field component measured at the same site at two different times when field values are different. We use the generalized notation $\mu_b = \Delta_1/\Delta_2$, where Δ_1 and Δ_2 are defined as numerator and denominator, respectively, of either Eq. (1), (2), or (3).

Rela . e magnetic permeability results

To solve for bulk relative permeability of the moon we perform a regression analysis on the generalized field-difference parameters Δ_1 and Δ_2, shown in Fig. 7. This curve has been constructed using over 2000 simultaneous Apollo 15 and Apollo 16 magnetometer data sets, measured during five orbits of the moon through the geomagnetic tail. These data have been carefully selected to eliminate data measured in the plasma sheet or contaminated by other induction modes such as eddy current induction (see Parkin *et al.*, 1974).

Effects of plasma diamagnetism and confinement are minimized by eliminating data points for which the magnitude of the external magnetizing field $H < 7 \times 10^{-5}$ Oe. Since poloidal eddy current induction is dependent upon time rate of change of H, inclusion of poloidal fields is minimized by averaging over 10-min intervals during which Apollo 15 and 16 data peak-to-peak variations are small. Then pairs of data points are selected from different times, using criteria to insure that the denominators in Eqs. (1) to (3) are non-zero. Finally, a regression analysis is performed on the set of ordered pairs (Δ_1, Δ_2) plotted in Fig. 7. The least-squares best estimate of the slope, calculated using the method of York (1966), is $\mu_b = 1.008 \pm 0.005$.

Lunar magnetic permeability results adjusted for ionospheric effects

We have calculated a value for relative magnetic permeability of the moon. To determine the absolute lunar permeability and iron abundance in the moon, we

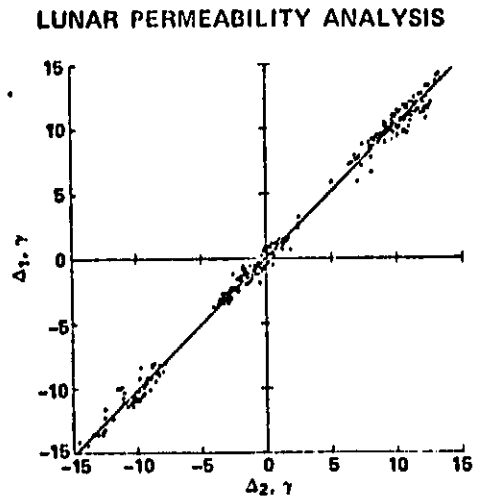

Fig. 7. Lunar permeability analysis, using all three vector axes of simultaneous Apollo 15 and 16 surface magnetometer data for five lunations in the geomagnetic tail lobes. The least-squares slope gives a value for the bulk lunar relative permeability: 1.008 ± 0.005. The parameters Δ_1 and Δ_2 are defined in the text.

consider the magnetic permeability of the environment exterior to the moon, in particular, the lunar ionosphere in the geomagnetic tail.

The lunar atmosphere (see Johnson, 1971; Hodges *et al.*, 1974) is the source of the ionosphere. The lunar atmosphere is an exosphere whose sources are neutralized solar-wind ions and neutral atoms outgassed from the moon. The species of solar-wind origin are ^{36}Ar, ^{20}Ne, ^{4}He, H_2, and H. Hydrogen and helium escape thermally with lifetimes ranging from 10^3 to 10^5 sec while ^{36}Ar and ^{20}Ne have much longer lifetimes which are controlled by photoionization.

Previous work on the lunar ionosphere has been confined to time periods when the moon is in the solar wind (Manka, 1972; Vondrak and Freeman, 1974). During the four-day period when the moon is in the geomagnetic tail, the solar wind is no longer a primary source of neutral atmosphere. He, H_2, and H thermally escape within several hours and do not contribute significantly to the lunar ionosphere. ^{20}Ne, ^{36}Ar, and ^{40}Ar are the main atmospheric constituents due to their long residence times. The ionization of the atmosphere in the solar wind is dominated by charge exchange (Weil and Barasch, 1963), whereas in the geomagnetic tail the principal process is photoionization by ultraviolet radiation from the sun. In addition, acceleration by the motional electric field has been considered to be the principal loss mechanism for ionospheric particles when the moon is in the solar wind. In the geomagnetic tail, plasma conditions are different; thermal escape, electric field acceleration, and ballistic collision with the surface are possible loss mechanisms.

The photoionization of the sunlit lunar atmosphere is determined by the solar spectrum and the photoproduction cross sections of each species. In this photoionization process the photon energy is used to ionize the neutral atoms and

the excess energy is converted to photoelectron kinetic energy. By considering the peak photon flux and cross sections, we estimate the photoelectron energy to be about 20 eV for both Ne and Ar. We assume that the ions remain at the effective temperature of the neutral atmosphere which is in thermal equilibrium with the surface at 300°K. The thermal speeds of the high energy electrons are in excess of the escape velocity (2.4×10^8 cm/sec). However, the electrons are also electrically attracted to the ions which are gravitationally bound to the moon at the low temperature of 300°K. To consider these competing effects we consider the equations governing the behavior of both the ions and electrons of each ionized species:

$$\frac{1}{n^+}\frac{dn^+}{dz} = \frac{-g(r)m^+}{kT^+} + \frac{eE}{kT^+} \tag{4}$$

$$\frac{1}{n_e}\frac{dn_e}{dz} = \frac{-g(r)m_e}{kT_e} - \frac{eE}{kT_e} \tag{5}$$

where n^+, m^+, T^+, and n_e, m_e, T_e are the density, mass, and temperature of the ions and electrons, respectively; z is altitude above the lunar surface; $g(r)$ is the lunar gravitational acceleration; e is charge on the electron; and k is Boltzmann's constant. The electric field E is the Rosseland field, which is responsible for maintaining local charge neutrality. Since $g(r)$ takes into account the finite mass of the lunar atmosphere, solution of Eqs. (4) and (5) for the density is valid far from the moon as well as near the lunar surface. A scale height can be calculated from this distribution which depends, for the model described above, on the ion mass and the electron temperature and is about 1100 km for both neon and argon. Using an expression given by Johnson (1971) for the mean residence time τ, we can now estimate the loss rate of the ionosphere by thermal escape. We also calculate the production rate for the ionospheric constituents. Using this information we then calculate the time derivative of the ion density:

$$\frac{dn}{dt} = p - n/\tau \tag{6}$$

where p is the production rate and n/τ is the loss rate. At equilibrium $n = p\tau$.

Results indicate a characteristic ion density of approximately 10 cm^{-3} between the surface and 100-km altitude. The energy density of this ionospheric plasma is dominated by the energetic electrons, and the geomagnetic tail field is about 10 gammas. The ionospheric plasma diamagnetic permeability μ_i is derived from $\mathbf{B} = \mu\mathbf{H} = \mathbf{H} + 4\pi\mathbf{M}$, where $\mathbf{M} = -nkT\mathbf{B}/B^2$:

$$\mu_i = (1 + \beta/2)^{-1} \tag{7}$$

where $\beta = 8\pi nkT/B^2$. Using ion density $n = 10$ ions/cm^3, plasma temperature $T \cong T_e = 1.5 \times 10^5$°K and $B = 10$ gammas, we calculate the ionospheric relative magnetic permeability to be $\mu_i = 0.8$. This theoretical diamagnetic permeability for the ionosphere compares favorably with the experimental value obtained by simultaneously considering our lunar relative permeability result and the experimental lunar induced dipole moment determined by Russell *et al.* (1974a). A

two-layer (ionosphere-moon) model is used to calculate permeability of the moon and the ionosphere relative to free space (see Parkin *et al.*, 1974). The ionosphere diamagnetic permeability is calculated to be $\mu_i = 0.76^{+0.11}_{-0.10}$ and the paramagnetic permeability of the moon, adjusted for ionospheric effects, is $\mu = 1.012^{+0.011}_{-0.008}$. This result is in general agreement with previous measurements using Explorer 35 and Apollo 12 magnetometer data reported by Parkin *et al.* (1974).

Iron abundance

Using the value of global lunar magnetic permeability, we can determine free iron and total iron abundances. The free and total iron values are also constrained by lunar density and moment of inertia, and are functions of thermal and compositional models of the lunar interior.

The lunar bulk permeability $\mu = 1.012^{+0.011}_{-0.008}$ is too high to be accounted for by any paramagnetic mineral which is a likely constituent of the lunar interior, implying that some material inside the moon must be in the ferromagnetic state. Assuming the ferromagnetic material is free iron of noninteracting multidomain grains, the lunar free iron abundance can be determined using a thermal model of the lunar interior. The thermal profile is approximated by a two-layer model with the boundary located at the iron Curie point isotherm. Figures 8 and 9 show free iron abundance (q) and total iron abundance (Q) related to ($\mu - 1$) and thermal profile. Q is shown for two compositional models; we assume the moon is composed of a homogeneous mineral (olivine or orthopyroxene) of uniform density 3.34 g/cm^3, with free iron grains disbursed uniformly throughout the sphere. All assumptions and the theoretical formulation leading to Figs. 8 and 9 are outlined in Appendix B. Using the temperature profiles shown in Fig. 6, we find that the iron Curie isotherm radius R_c should be in the range $\lambda \geq 0.88$, where $\lambda = R_c/R_m$. In our calculations we use $\lambda = 0.88$.

Without adjusting our measured bulk permeability for ionospheric effects we determine free iron abundance to be 1.6 ± 1.0 wt.%. This corresponds to a total iron abundance of 6.7 ± 0.6 wt.% for the free iron/olivine model and 13.2 ± 0.4 wt.% for the free iron/orthopyroxene model. Using $\mu = 1.012^{+0.011}_{-0.008}$, which does account for the lunar ionosphere, we determine free iron abundance to be $2.5^{+2.3}_{-1.7}$ wt.%. The free iron abundance corresponds to total iron abundance of 6.0 ± 1.0 wt.% for the free iron/olivine lunar model, or 12.5 ± 1.0 wt.% for the free iron/orthopyroxene model. If we assume the lunar composition to be one or a combination of these minerals, the total iron abundance will be between 5.0 and 13.5 wt.%.

Summary and Conclusions

Lunar electrical conductivity and temperature

(1) Conductivity results presented in this paper have been determined using a new transient-superposition technique which increases the data signal-to-noise

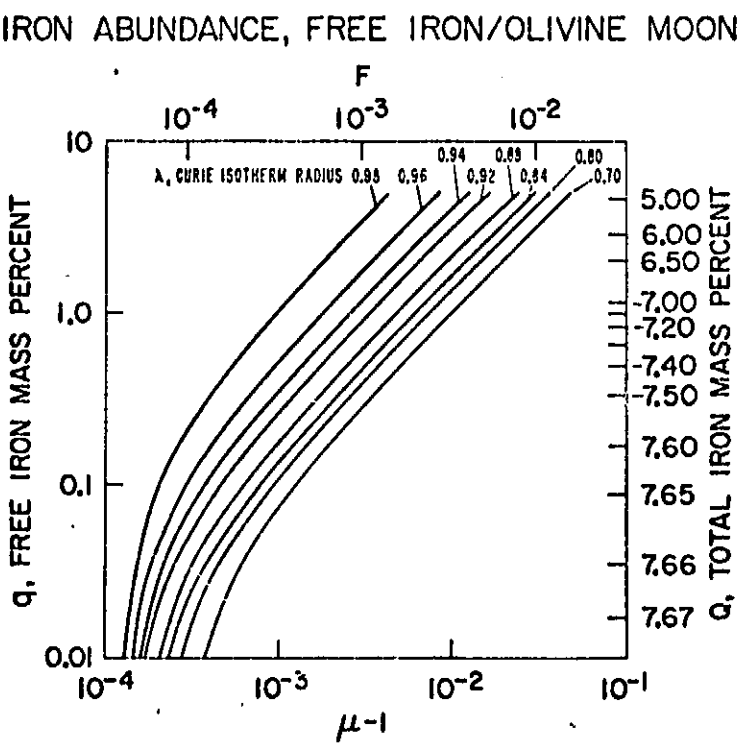

Fig. 8. Free and total iron abundances in the moon as a function of the bulk magnetic permeability μ and temperature profile of the moon, for a free iron/olivine compositional model.

ratio and uses both radial and tangential response data in the geomagnetic tail lobes.

(2) The average bulk electrical conductivity of the moon is calculated to be 7×10^{-4} mho/m.

(3) The calculated radially varying conductivity profile (see Fig. 4) rises rapidly with depth to $\sim 10^{-1}$ mho/m within the first 250 km, then remains relatively constant to 800-km depth.

(4) The limiting maximum size of a highly conducting core ($\geq 7 \times 10^{-3}$ mho/m) is calculated to be $\leq 0.57 R/R_{moon}$; that is, our present resolution allows us to probe to depths where moonquake foci have been located by seismic studies.

(5) A conversion of electrical conductivity to temperature using the data of Duba *et al.* (1974) for olivine yields a thermal profile which is relatively hot, implying that the Curie point is within 200 km of the lunar surface.

Lunar magnetic permeability and iron abundance

(1) Magnetic permeability results have been obtained using simultaneous data from the Apollo 15 and 16 surface magnetometers and requiring no orbital

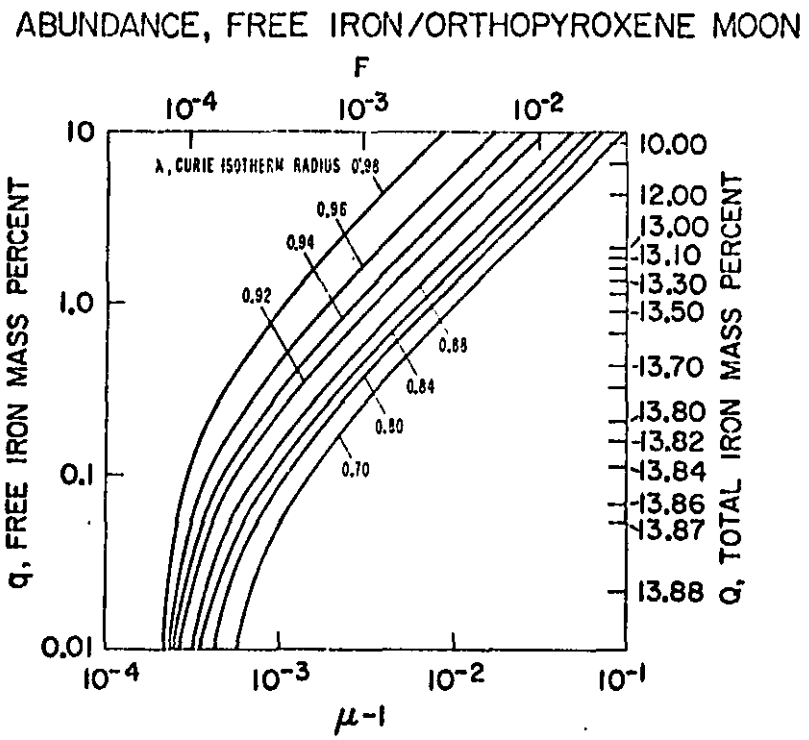

Fig. 9. Free and total iron abundances in the moon for a free iron/orthopyroxene lunar model.

magnetic field data. Both radial and tangential magnetic data are used in the analysis.

(2) The bulk magnetic permeability of the moon relative to its environment is calculated directly from magnetometer data to be $\mu_b = 1.008 \pm 0.005$.

(3) The lunar ionosphere in the geomagnetic tail is modeled, and theoretical calculations yield an ionospheric permeability of 0.8, a value consistent with surface and orbital magnetometer measurements.

(4) The magnetic permeability of the moon, adjusted for effects of its diamagnetic environment, is calculated to be $\mu = 1.012^{+0.011}_{-0.008}$.

(5) Free iron abundance is determined from our permeability and temperature calculations to be $2.5^{+3}_{-1.7}$ wt.%.

(6) Total iron abundance is found for two compositional models of the moon: free iron/olivine model, 6.0 ± 1.0 wt.%; free iron/orthopyroxene model, 12.5 ± 1.0 wt.%. Assuming the moon is composed of one or a combination of these minerals, the overall iron abundance will be between 5.0 and 13.5 wt.%.

Acknowledgments—The authors are especially grateful to James Arvin and Karen Neier of Computer Sciences Corporation for their diligence in rapidly developing the IMLAC programs necessary for the present analysis. We wish to thank Dr. William Barker of the University of Santa Clara and Dr.

Thomas Mucha of CSC for their theoretical work on properties of the lunar ionosphere. And once again we thank Marion Lepg and her coworkers at Adia Interim Services for their excellent data reduction services. We are pleased to acknowledge research support for C. W. P. under NASA grant number NGR-05-017-027 and for W. D D. under NASA grant number NGR-45-001-040.

REFERENCES

Akimeto S., Horai K., and Boku T. (1958) Magnetic susceptibility of orthopyroxenes. *J. Geomag. Geoelect.* 10, 7–11.

Anderson K. A. (1965) Energetic electron fluxes in the tail of the geomagnetic fiel.. *J. Geophys. Res.* 70, 4741–4763.

Backus G. and Gilbert F. (1970) Uniqueness in the inversion of inaccurate gross earth data. *Phil. Trans. Roy. Soc.* A266, 123.

Bozorth R. M. (1951) *Ferromagnetism.* D. Van Nostrand.

Dana E. S. (1966) *Textbook of Mineralogy.* 4th edition by W. E. Ford. John Wiley & Sons.

Deer W. A., Howie R. A., and Zussman J. (1962) *Rock-forming Minerals.* John Wiley Co.

Duba A. and Ringwood A. E. (1973) Electrical conductivity, internal temperatures and thermal evolution of the moon. *The Moon* 7, 356.

Duba A., Heard H. C., and Schock R. N. (1972) The lunar temperature profile. *Earth Planet. Sci. Lett.* 15, 301.

Duba A., Heard H. C., and Schock R. N. (1974) Electrical conductivity of olivine at high pressure and under controlled oxygen fugacity. *J. Geophys. Res.* 79, 1667.

Dyal P. and Parkin C. W. (1971a) Electrical conductivity and temperature of the lunar interior from magnetic transient-response measurements. *J. Geophys. Res.* 76, 5947.

Dyal P. and Parkin C. W. (1971b) The Apollo 12 magnetometer experiment: Internal lunar properties from transient and steady magnetic field measurements. *Proc. Lunar Sci. Conf. 2nd*, p. 2391–2413.

Dyal P., Parkin C. W., and Sonett C. P. (1970) Lunar surface magnetometer. *IEEE Trans. on Geoscience Electronics GE-8(4)*, 203–215.

Dyal P., Parkin C. W., and Cassen P. (1972) Surface magnetometer experiments: Internal lunar properties and lunar surface interactions with the solar plasma. *Proc. Lunar Sci. Conf. 3rd*, p. 2287–2307.

Dyal P., Parkin C. W., and Daily W. D. (1973) Surface magnetometer experiments: Internal lunar properties. *Proc. Lunar Sci. Conf. 4th*, p. 2229–2945.

Dyal P., Parkin C. W., and Daily W. D. (1974) Temperature and electrical conductivity of the lunar interior from magnetic transient measurements in the geomagnetic tail. *Proc. Lunar Sci. Conf. 5th*, p. 3059–3071.

England A. W., Simmons G., and Strangway D. (1968) Electrical conductivity of the moon. *J. Geophys. Res.* 73, 3219.

Hanks T. C. and Anderson D. L. (1972) Origin, evolution and present thermal state of the moon. *Phys. Earth Planet. Interiors* 5, 409–425.

Hobbs B. A. (1973) The inversion problem of the moon's electrical conductivity. *Earth Planet. Sci. Lett.* 17, 380–384.

Hodges R. R., Hoffman J. H., and Johnson F. S. (1974) The lunar atmosphere. *Icarus* 21, 415–426.

Johnson F. S. (1971) Lunar atmosphere. *Rev. Geophys. Space Phys.* 9, 813–823.

Khitarov N. I., Slutskiy A. B., and Pugin V. A. (1970) Electrical conductivity of basalts at high T-P and phase transitions under upper mantle conditions. *Phys. Earth Planet. Interiors* 3, 334–342.

Kuckes A. F. (1974) Lunar magnetometry and mantle convection. *Nature* 252, 670–672.

Manka R. H. (1972) The lunar atmosphere and ionosphere. Ph.D. Dissertation, Department of Space Science, Rice University, Houston, Texas.

Nagata T. (1961) *Rock Magnetism.* Maruzen Co. Ltd.

Nagata T., Yukutake T., and Uyeda S. (1957) On magnetic susceptibility of olivines. *J. Geomag. Geoelect.* 9, 51–56.

Nakamura Y., Latham G., Lammlein D., Ewing M., Duennebier F., and Dorman J. (1974) Deep lunar interior from recent seismic data. *Geophys. Res. Lett.* **1**, 137–140.
Olhoeft G. R., Frisillo A. L., Strangway D. W., and Sharpe H. (1973) Electrical properties of lunar solid samples (abstract). In *Lunar Science IV*, p. 575–577. The Lunar Science Institute, Houston.
Parkin C. W., Dyal P., and Daily W. D. (1973) Iron abundance in the moon from magnetometer measurements. *Proc. Lunar Sci. Conf. 4th*, p. 2947–2961.
Parkin C. W., Daily W. D., and Dyal P. (1974) Iron abundance and magnetic permeability of the moon. *Proc. Lunar Sci. Conf. 5th*, p. 2761–2778.
Phillips R. J. (1972) The lunar conductivity profile and the nonuniqueness of electromagnetic data inversion. *Icarus* **17**, 88–103.
Presnall D. C., Simmons C. L., and Porath H. (1972) Changes in electrical conductivity of a synthetic basalt during melting. *J. Geophys. Res.* **77**, 5665–5672.
Ringwood A. E. and Essene E. (1970) Petrogenesis of lunar basalts and the internal constitution and origin of the moon. *Science* **167**, 607–610.
Russell C. T., Coleman P. J. Jr., Lichtenstein B. R., and Schubert G. (1974a) The permanent and induced magnetic dipole moment of the moon. *Proc. Lunar Sci. Conf. 5th*, p. 2747–2760.
Russell C. T., Coleman P. J. Jr., and Schubert G. (1974b) Lunar magnetic field: Permanent and induced dipole moments. *Science* **186**, 825–826.
Schwerer F. C., Huffman G. P., Fisher R. M., and Nagata T. (1972) D. C. electrical conductivity of lunar surface rocks. *The Moon* **4**, 187.
Sonett C. P., Colburn D. S., Currie R. G., and Mihalov J. D. (1967) The geomagnetic tail; topology, reconnection and interaction with the moon. In *Physics of the Magnetosphere* (editors R. L. Carovillano, J. F. McClay, and H. R. Radoski), p. 380. D. Reidel.
Tebble R. S. and Craik D. J. (1969) *Magnetic Materials*. Wiley-Interscience, p. 107.
Vondrak R. R. and Freeman J. W. (1974) The lunar ionosphere. Conf. on Interactions of the Solar Wind with the Ancient and Modern Moon. (abs.), Williams Bay, Wisconsin, 1–3.
Weil H. and Barasch M. L. (1963) A theoretical lunar ionosphere. *Icarus* **1**, 346–356.
York D. (1966) Least-squares fitting of a straight line. *Canadian J. Phys.* **44**, 1079–1086.

Appendix A

It has been shown by Parkin *et al.* (1973) that the field on the surface of a spherically symmetric two-layer magnetically permeable sphere can be expressed as:

$$\mathbf{B} = H_x(1+2F)\hat{x} + H_y(1-F)\hat{y} + H_z(1-F)\hat{z} \tag{1}$$

where

$$F = \frac{(2\eta+1)(\mu_1-1) - \lambda^3(\eta-1)(2\mu_1+1)}{(2\eta+1)(\mu_1+2) - 2\lambda^3(\eta-1)(\mu_1-1)} \tag{2}$$

Here **H** is the field external to the sphere at large distances; $\eta = \mu_1/\mu_2$; μ_1 and μ_2 are relative magnetic permeability of the shell and core respectively (permeability of free space $\mu_0 = 1$); $\lambda = R_2/R_1$ where R_2 is the radius of the boundary between the two permeable regions and R_1 is the radius of the sphere. As applied to the lunar sphere Eq. (1) is expressed in the ALSEP coordinate system which has its origin on the lunar surface. The x axis is directed radially outward from the surface; the y and z axes are tangential to the surface, directed eastward and northward, respectively.

In order to measure the dipole induced in the moon by the external field **H** we subtract two values of **B** in Eq. (1) for which **H** is different: $\Delta\mathbf{B} = \mathbf{B} - \mathbf{B}'$. Forming this difference at two different points on the moon for the two values of the external field we have in component form:

$$\begin{aligned} \Delta B_x &= (1+2F)\Delta H_x \\ \Delta B_y &= (1-F)\Delta H_y \\ \Delta B_z &= (1-F)\Delta H_z \end{aligned} \tag{3}$$

where $i = 1, 2$ for the two different magnetometer sites. The two fields $\mathbf{H}_i$ can be related by the transformation

$$\begin{aligned} \mathbf{H}_2 &= |\mathrm{A}|\mathbf{H}_1 \\ \mathbf{H}_1 &= |\mathrm{A}|^{-1}\mathbf{H}_2 \end{aligned} \tag{4}$$

where $|A|$ is the transformation matrix relating the ALSEP coordinate systems at the two sites. Equations (3) and (4) can be solved simultaneously eliminating $\mathbf{H}_i$ to give

$$\begin{aligned} \Delta B_{2x} &= (1+2F)\left[a_{11}\frac{\Delta B_{1x}}{(1+2F)} + a_{12}\frac{\Delta B_{1y}}{(1-F)} + a_{13}\frac{\Delta B_{1z}}{(1-F)}\right] \\ \Delta B_{2y} &= (1-F)\left[a_{21}\frac{\Delta B_{1x}}{(1+2F)} + a_{22}\frac{\Delta B_{1y}}{(1-F)} + a_{23}\frac{\Delta B_{1z}}{(1-F)}\right] \\ \Delta B_{2z} &= (1-F)\left[a_{31}\frac{\Delta B_{1x}}{(1+2F)} + a_{32}\frac{\Delta B_{1y}}{(1-F)} + a_{33}\frac{\Delta B_{1z}}{(1-F)}\right] \end{aligned} \tag{5}$$

where a_{ij} are the elements of $|A|$. From Eqs. (5) we have three expressions involving the induced magnetic moment HR_1^3F which are:

$$\begin{aligned} \mu_b &= \frac{\Delta B_{2x} - a_{11}\Delta B_{1x}}{a_{12}\Delta B_{1y} + a_{13}\Delta B_{1z}} \\ \mu_b &= \frac{a_{21}\Delta B_{1x}}{\Delta B_{2y} - a_{22}\Delta B_{1y} - a_{23}\Delta B_{1z}} \\ \mu_b &= \frac{a_{31}\Delta B_{1x}}{\Delta B_{2z} - a_{32}\Delta B_{1y} - a_{33}\Delta B_{1z}} \end{aligned} \tag{6}$$

with

$$\mu_b = \frac{1+2F}{1-F} \tag{7}$$

since Eqs. (5) could have been expressed with ΔB_i as the dependent variable, Eqs. (6) can also be written interchanging 1 and 2 subscripts on the ΔB quantities and using the matrix elements of $|A|^{-1}$ instead of those from $|A|$.

APPENDIX B

Limits imposed on μ of Eqs. (6) in Appendix A by the LSM data can be used to calculate the lunar iron abundance for suitable lunar compositional and thermal models. Two of the models are described, including magnetic and other geophysical constraints. In both cases the lunar interior is modeled by a sphere of homogeneous composition. Free iron of multidomain noninteracting grains is assumed to be uniformly distributed throughout a paramagnetic mineral. The paramagnetic component in one case is olivine $[y\mathrm{Fe_2SiO_4} \cdot (1-y)\mathrm{Mg_2SiO_4}]$ and in the other case is orthopyroxene $[y\mathrm{FeSiO_3} \cdot (1-y)\mathrm{MgSiO_3}]$. The free iron is ferromagnetic in the regions where the temperature T is less than the iron Curie temperature T_c, and it is paramagnetic where $T > T_c$. Therefore, each model is a two layer permeable sphere where μ_1 and μ_2 are the relative magnetic permeability of the spherically symmetric shell and core respectively; R_2 is the core-shell boundary. [Equation (2) of Appendix A relates these variables to the measured magnetic moment HR_1^3F.] We consider the magnetic contributions from both free and combined iron in both the shell and core of the model with $\mu_{1,2} = 1 + 4\pi K_{1,2}$ where

$$\begin{aligned} K_1 &= K_p(y, T_1) + K_F(q) \\ K_2 &= K_p(y, T_2) + K_F(q) \end{aligned} \tag{1}$$

and K_p is the paramagnetic susceptibility of the olivine or orthopyroxene, y is the mole fraction of ferrosilicate in the mineral, T_1 is the uniform temperature of the shell, T_2 is the uniform temperature of

the core, K_r is the apparent ferromagnetic susceptibility of free iron in emu/cm^3, K'_r is the apparent paramagnetic susceptibility of free iron (above the Curie temperature), and q is the mass fraction of free iron in the moon.

The measured susceptibility of the free iron K_r is an apparent value which differs from the intrinsic susceptibility of iron K because of self-demagnetization of the iron grains and the fraction of iron in the moon. The apparent and intrinsic susceptibility of the free iron are related (see Nagata, 1961) by

$$K_r = \frac{q\rho}{\rho_r} \frac{K}{1 + NK} \tag{2}$$

where ρ is the lunar density (assumed uniform throughout the moon), and ρ_r is the density of iron. An analogous expression relates K'_r, the apparent paramagnetic susceptibility, and K', the intrinsic paramagnetic susceptibility of free iron ($T > T_c$).

Nagata *et al.* (1957) found the susceptibility of olivine to be $2.4y \times 10^{-3}$ emu/mole at room temperature. Using this expression, the Curie law temperature dependence, and the following empirical equation for olivine density (Dana, 1966)

$$\rho_p(y) = 0.94y + 3.26 \text{ g/cm}^3, \tag{3}$$

we obtain for olivine

$$K_r = 0.14 \frac{y}{T} \frac{46y + 158}{63y + 141} \text{ emu/cm}^3. \tag{4}$$

Similarly Akimoto *et al.* (1958) give the susceptibility for pyroxenes: $1.1y \times 10^{-2}$ emu/mole. From Deer *et al.* (1962) we obtain the following empirical expression for pyroxene density:

$$\rho_p(y) = 0.71y + 3.15 \text{ g/cm}^3. \tag{5}$$

Again, combining the expressions from Akimoto *et al.* and Deer *et al.* with the Curie law temperature dependence, we obtain for pyroxene

$$K_r = 0.095 \frac{y}{T} \frac{24y + 108}{32y + 100} \text{ emu/cm}^3. \tag{6}$$

The lunar moment of inertia is approximately that of a sphere of uniform density (Ringwood and Essene, 1970). Choosing a uniform density for our lunar model we can write

$$\frac{1}{\rho} = \frac{q}{\rho_r} + \frac{1 - q}{\rho_p(y)} \tag{7}$$

The free iron abundance q can be determined as a function of μ for the orthopyroxene/free iron model by simultaneously solving Eqs. (2) and (7) of Appendix A and Eqs. (1), (2), (5), (6), and (7) above. The olivine/free iron model solution is determined by solving Eqs. (2) and (7) of Appendix A and Eqs. (1), (2), (3), (4), and (7) above. Results for iron abundances as a function of lunar magnetic permeability are given in Figs. 8 and 9. Q, the fractional lunar mass due to both chemically uncombined and combined iron, is constrained by q and the lunar density. For the orthopyroxene/free iron model

$$Q = q + \frac{56y}{32y + 100}(1 - q) \tag{8}$$

and for the olivine/free iron model

$$Q = q + \frac{112y}{64y + 140}(1 - q). \tag{9}$$

In Eqs. (8) and (9) y can be eliminated by substitution of Eqs. (3), (5), and (7); therefore, the total iron and free iron abundances are directly related. Figures 8 and 9 show the results of these calculations relating q, Q and $\mu - 1$.

Constants used in the calculations for both models are:

uniform density of moon	$\rho = 3.34$ g/cm^3
density of free iron	$\rho_F = 7.85$ g/cm^3
demagnetization factor of iron grains	$N = 3.5$ (Nagata, 1961)
initial intrinsic ferromagnetic susceptibility of iron	$K = 12$ emu/cm^3 (Bozorth, 1951)
intrinsic paramagnetic susceptibility of iron	$K' = 2.2 \times 10^{-4}$ emu/cm^3 (Tebble and Craik, 1969)
thermal models	$T_1 = 900$°K, $T_2 = 1700$°K, $\lambda = 0.98, 0.96, 0.94, 0.92$
	$T_1 = 800$°K, $T_2 = 1600$°K, $\lambda = 0.88, 0.84$
	$T_1 = 700$°K, $T_2 = 1400$°K, $\lambda = 0.80$
	$T_1 = 600$°K, $T_2 = 1000$°K, $\lambda = 0.70$

Publ. in Lunar Science VII, part I, 1976.

STRUCTURE OF THE LUNAR INTERIOR FROM MAGNETIC FIELD MEASUREMENTS,

P. Dyal*, C.W. Parkin**, and W.D. Daily***.
*NASA-Ames Research Center, Moffett Field, CA 94035
**Univ. of Santa Clara, Santa Clara, CA 95053
***Eyring Research Institute, Provo, UT 84601

The electrical conductivity and magnetic permeability of the lunar interior have been determined from measurements by a total of six lunar surface and orbiting magnetometers. From these results, characteristics of lunar internal structure are inferred.

A new technique has been applied to conductivity analysis in which simultaneous data is used from a network of three instruments: The Apollo 15 lunar surface magnetometer (LSM), the Apollo 16 LSM, and the Apollo 16 subsatellite magnetometer, which provides coverage around the entire global circumference. Also, a two-instrument technique has been applied which uses Apollo 12 LSM data and simultaneous data from the Goddard magnetometer aboard Explorer 35. All measurements are made when the moon is located in high-latitude regions of the geomagnetic tail where plasma effects in the lunar environment are minimal. Individual magnetic events are superimposed to obtain a single large transient for analysis. Also, during examination of five years of data one exceptionally large, well-behaved transient was recorded when the moon was in the geomagnetic tail. This single event allowed substantial improvement in resolution and sounding depth for conductivity analysis.

Although the two types of conductivity analysis are analytically different and use measurements obtained over a five-year period from six different magnetometers, results are in surprisingly close agreement. The conductivity profile result is shown in the accompanying figure. A striking feature is the abrupt transition near 300 km depth where a knee occurs in the conductivity profile. The conductivity increases rapidly from the surface to about 4×10^{-3} mhos/m at 300 km depth. At greater depths the conductivity increases more slowly to about 2×10^{-2} mhos/m at 800 km depth.

This conductivity transition at 300 km depth, the location of which corresponds closely to that of the seismic velocity change reported by Nakamura et al. (1974), strongly implies a structural or compositional change at that depth.

In addition, the lunar magnetic permeability determined from magnetometer measurements has been used to place limits on a possible highly conducting core in the moon. In the permeability analysis the moon is represented by a three-layer magnetic model: an outer shell of temperature (T) below the Curie point (T_c), whose permeability μ is dominated by ferromagnetic free iron; an intermediate shell of $T > T_c$ where permeability $\approx \mu_o$, that of free space; and a highly conducting core ($\sigma >> 10^{-2}$ mhos/m) modeled by $\mu = 0$. This core effectively excludes external magnetic fields over time lengths of days and therefore acts as a strongly diamagnetic region ($\mu \rightarrow 0$).

A theoretical analysis has been carried out to relate the induced magnetic dipole moment to the core size. The induced dipole moment has been determined from simultaneous Apollo 12 and Ames Explorer measurements to be $2.1 \times 10^{18} \pm 1.0 \times 10^{18}$ gauss cm^3 (Parkin et al., 1974) and from simultaneous Apollo 15 and 16 measurements to be $1.4 \times 10^{18} \pm 0.9 \times 10^{18}$ gauss cm^3 (Dyal et al., 1975).

Results show that the core size is a function of the depth of the Curie isotherm and lunar composition. To calculate an upper limit on core size, we assume that the compositional mineral of the moon has no iron silicate and take an extreme depth of 350 km for the Curie point (Toksöz et al., 1974) so that free iron content is maximized. Then the maximum allowable core size is 470 km for an olivine moon and 600 km for an orthopyroxene moon. However, both magnetic permeability and electrical conductivity analyses are consistent with the absence of a highly conducting lunar core.

REFERENCES

Dyal, P., Parkin, C.W., and Daily, W.D., 1975, Proc. Lunar Sci. Conf. 6th, p. 2909-2926.

Nakamura, Y., Latham, G., Lammlein, D., Ewing, M., Duennebier, F., and Dorman, J., 1974, Geophys. Res. Lett., 1, p. 137-140.

Parkin, C.W., Daily, W.D., and Dyal, P., 1974, Proc. Lunar Sci. Conf. 5th, p. 2761-2778.

Toksöz, M.N., Dainty, A.M., Solomon, S.C., and Anderson, K.R., 1974, Rev. Geophys. Space Phys., 12, p. 539-567.

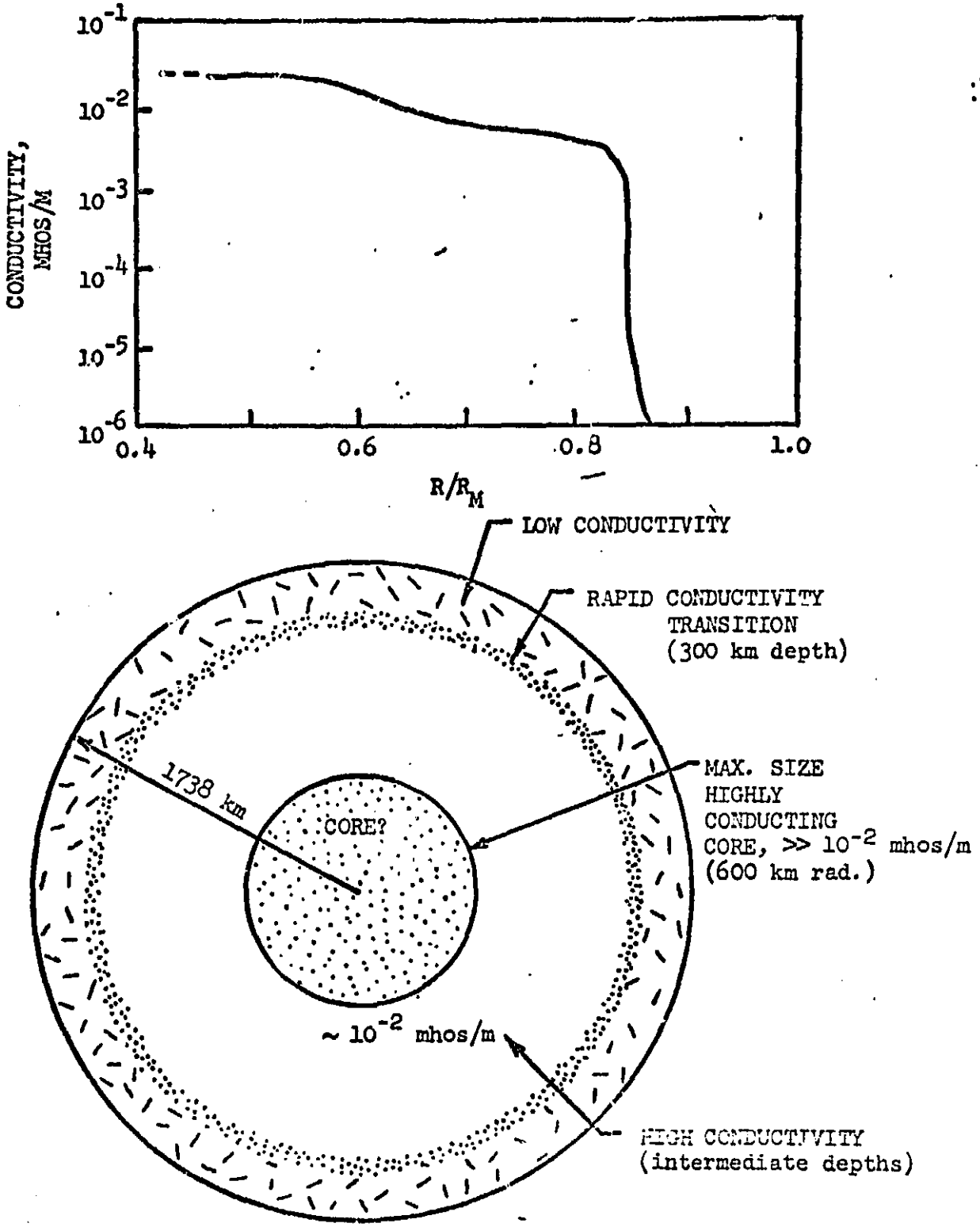

To be publ. in EOS, vol. 57, 1976.

LUNAR ELECTRICAL CONDUCTIVITY PROFILE FROM MAGNETOMETER NETWORK

W. D. Daily (Eyring Research Institute, Provo, UT 84601)
P. Dyal (NASA-Ames Research Center, Moffett Field, CA 94035)
C. W. Parkin (University of Santa Clara, Santa Clara, CA 95053)

The electrical conductivity of the lunar interior has been determined with a new analytical technique in which simultaneous data are used from a network of the lunar magnetometers: the Apollo 15 lunar surface magnetometer (LSM), the Apollo 16 LSM, and the Apollo 16 subsatellite magnetometer. From this network measurements of induced poloidal fields can be made over the lunar sphere, which are therefore representative of the whole-moon electrical current distribution. Magnetic field measurements were made during times when the moon was at high latitudes in the geomagnetic tail lobes. Since in the lobes the plasma effects are minimal, the moon has been modeled as a sphere in a vacuum. In the analysis many individual magnetic events are superimposed to obtain a single large transient with much better signal-to-noise characteristics than single events. The conductivity profile obtained from this 3-magnetometer technique is in close agreement with previous results from our 2-magnetometer analysis using the Apollo 12 LSM and Explorer 35 magnetometers. The conductivity increases rapidly from the surface to about 4×10^{-3} mhos/m at 300 km depth. At greater depths the conductivity increases more slowly to about 2×10^{-2} mhos/m at 800 km depth. A striking feature of the profile is the abrupt transition near 300 km depth where a knee occurs in the conductivity profile. This conductivity transition, the location of which corresponds closely to that of the lunar seismic velocity change reported by Nakamura et al. (1974), strongly implies structural or compositional changes at that depth.